Available online at www.sciencedirect.com

ScienceDirect

Procedia IUTAM 14 (2015) 303 – 310

Procedia IUTAM

www.elsevier.com/locate/procedia

IUTAM_ABCM Symposium on Laminar Turbulent Transition

Effect of freestream turbulence on roughness-induced crossflow instability

Seyed M. Hosseini[a,*], Ardeshir Hanifi[a,b], Dan S. Hennigson[a]

[a] *KTH Royal Institute of Technology, Department of Mechanics, Linné Flow Centre, SeRC, SE-100 44 Stockholm, Sweden*
[b] *Swedish Defence Research Agency, FOI, SE-164 90 Stockholm, Sweden*

Abstract

The effect of freestream turbulence on generation of crossflow disturbances over swept wings is investigated through direct numerical simulations. The set up follows the experiments performed by Downs et al. (2012). In these experiments the authors use ASU(67)-0315 wing geometry which promotes growth of crossflow disturbances. Distributed roughness elements are locally placed near the leading edge with a given spanwise wavenumber to excite the corresponding stationary crossflow vortices. In present study, we partially reproduce the isotropic homogenous freestream turbulence through direct numerical simulations using freestream spectrum data from the experiments. The generated freestream fields are then applied as the inflow boundary condition for direct numerical simulation of the wing. The distributed roughness elements are modelled through wing surface deformation and placed near the leading edge to trigger the stationary crossflow disturbances. The effects of the generated freestream turbulence on the initial amplitudes and growth of the boundary layer perturbations are then studied.

Selection and peer-review under responsibility of ABCM (Brazilian Society of Mechanical Sciences and Engineering)

Keywords:

1. Introduction

A conventional three-dimensional boundary layer on a wing has a certain number of instabilities. The usually dominant one is the so-called crossflow instability. It arises due to the inflectional crossflow velocity component in the boundary layer. In such flows, a negative pressure gradient has a destabilising effect leading to the growth of cross flow vortices on the upper side of the wing, particularly in a negative angle of attack. The growth rate is mainly dictated by the flow configuration, while the excited initial amplitude is dependent on a multitude of factors. For instance, freestream turbulence, surface roughness characteristics, and acoustic waves along with the receptivity characteristics of the flow determine the initial perturbation amplitude.

* Corresponding author. Tel.: +46-08-790-6876.
E-mail address: hosse@mech.kth.se

Selection and peer-review under responsibility of ABCM (Brazilian Society of Mechanical Sciences and Engineering)
doi:10.1016/j.piutam.2015.03.053

Numerous experiments have also been conducted to study the problem of boundary layer receptivity to freestream turbulence. In the experiments by Matsubara et al.[1], the authors further correlated the streaky structures with transient growth which is augmented by an increase in freestream turbulence levels. The presence of surface roughness can promote such effects. Moreover there exists a conjecture that a continuous receptivity process plays an important role in feeding the boundary layer perturbations in the streamwise direction. Jonáš et al.[2] investigated the effect of freestream turbulence length scale on a flat-plate bypass transition. Larger integral length scales showed to advance the transition location while keeping the level of turbulent intensity. Fransson et al.[3] studied the transition caused by freestream turbulence on a flat plate boundary layer. They introduce a transitional Reynolds number inversely proportional to $(Tu)^2$. Moreover Shahinfar et al.[5] studied the effect of varying turbulence intensities on boundary layers and correlate the Reynolds number of the transition location with the turbulence intensity.

Deyhle and Bippes[?] studied growth of perturbation in a three-dimensional boundary layer with emphasis on effects of environmental conditions. They report dominance of stationary crossflow vortices for low level of freestream turbulence, while find travelling crossflow perturbations being dominant at higher freestream turbulence. Kurian et al.[4] conducted experiments on a swept flat plate with a leading edge studying the receptivity of the three-dimensional boundary layer to freestream turbulence. They also confirm the previous observations that higher turbulence environments give way to dominance of travelling crossflow waves. Nevertheless, they showed that a linear mechanism prevails in the range of studied freestream turbulence intensities. Moreover, it was observed that above a certain threshold, increasing the turbulence intensities has no tangible effect on the growth of the travelling crossflow modes. Recently, Hunt,[6] conducted experiments regarding crossflow instability on a swept wing including detailed measurements of surface roughness quality, and freestream turbulence characteristics, such as frequency spectrum. In a continuation of this work, Downs[7] includes additional freestream information comprising of Taylor micro scales and integral length scales. In the study by Hunt[6], the effect of freestream turbulence at very low levels of freestream turbulence is examined. One counter intuitive observation was the transition delay by slightly increasing turbulence density at that low level range. Downs[7] covers a wider range in his study in terms of freestream turbulence intensities and length scales. The inclusion of detailed measurements of freestream turbulence length scales and spectrum provides invaluable information to properly quantify the receptivity characteristics of such boundary layers exclusively for numerical reproduction of the experimental conditions.

Jacobs et al.[8] for the first time followed the methodology proposed by Grosch et al.[9] to synthesize freestream turbulence. Their method allowed to skip over the simulation of the far-field and the leading edge. Later, Brandt et al.[10] followed a similar method to produce the synthetic turbulence as an inflow boundary condition to study the transition process in a boundary layer. They varied the energy spectrum of the generated synthetic field. Increasing the integral length scale moved the transition location to lower Reynolds numbers. Moreover, two mechanisms were found playing a major role in exciting the perturbations inside the boundary layer. A linear mechanism, the so called lift up effect, is dominant if low-frequency modes diffuse into the boundary layer. On the contrary, if the freestream perturbations are mainly located above the boundary layer a nonlinear process takes over and generates streamwise vortices inside the boundary layer. This method was further applied to a swept flat plate in the simulations by Schrader et al.[11], where stationary crossflow vortices are generated through roughness elements. They also confirm the results of experiments where a higher turbulent intensity promotes the dominance of travelling crossflow modes. The initial amplitude of the perturbations scales linearly with the level of turbulent intensity. Nevertheless, larger turbulent intensities amplifies the effect of non-linearities. Ovchinnikov et al.[12] included the leading edge of a flat plate in their study of receptivity of boundary layers to freestream turbulence perturbations. In their simulation the box was extended to the upstream. They generate the freestream perturbations similar to[8] but through including the Fourier modes instead of the Orr-Sommerfeld modes. They notice a strong dependency of the transition mechanism on turbulent integral length scale. In their simulations the turbulent intensity was kept at a fixed value of 6%.

In this study, the experimental set up by Downs[7] is considered in order to investigate the effect of freestream turbulence on crossflow dominated flows through direct numerical simulations. An array of roughness elements has been placed near the leading edge at the same location as the experiment. Periodic boundary conditions are used in the spanwise direction. The width in the spanwise direction is chosen such that the array of roughness elements has the same periodicity as in the experiment and approximately the same integral length scale. This will generate crossflow vortices which gain energy from the flow and grow in amplitude as the propagate downstream. Two test

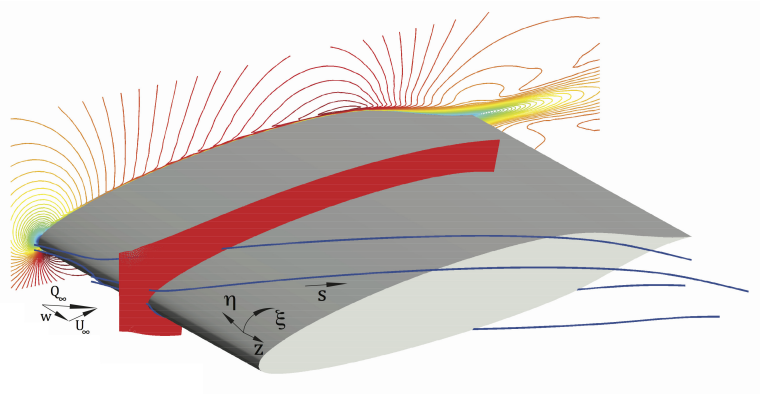

Fig. 1. Swept ASU(67)-0315 wing, with the incoming velocity Q_∞. The wing is at an angle of attack of $-2.9°$. (ξ, η, z) and (x, y, z) represent locally fitted curvilinear and cartesian coordinate systems respectively. (u_ξ, v_η, w) and (u, v, w) are the corresponding defined velocities in the introduced coordinates systems. The spectral elements for DNS are depicted in red. The normalized streamwise velocity contour lines from the RANS solution are shown ranging from 0.0 to 1.54 with a spacing of 0.024, which their values are used for the DNS baseflow. The blue lines represent the streamlines of the baseflow.

cases having turbulent intensities of 0.04% and 0.4% are selected. The perturbation fields are generated via direct numerical simulations and fed in on top up of the inflow boundary condition.

2. Direct numerical simulations

2.1. Numerical tool

Direct numerical simulations were performed using the incompressible Navier-Stokes solver 'Nek5000' by Fischer et al.[13], which uses the spectral element method proposed by Patera[14]. Enabling geometrical flexibility using finite element methods combined with the accuracy provided by spectral methods are the main advantages of using such codes. The spatial discretisation is obtained by decomposing the physical domain into spectral elements. The solution to the Navier-Stokes equations is approximated element-wise as a sum of Lagrange interpolants defined by an orthogonal basis of Legendre polynomials up to degree N. The following results have been obtained using $N = 11$.

2.2. Geometry and flow parameters

The geometry is a swept wing with cross-section corresponding to ASU(67)-0315 airfoil with a sweep angle of 45 degrees and angle of attack of -2.9 degrees. The Reynolds number based on the freestream velocity and streamwise chord length is 2.8×10^6. The portion of the wing that is simulated is chosen such that it includes all the interesting phenomena occurring on the wing, as depicted in figure 1. This entails the receptivity mechanism, initial perturbations growth, and the transition to turbulence. The upstream inflow is placed far upstream of the wing to rule out any numerical artifacts near the leading edge following the studies by Tempelmann et al.[15,16]. The upper bound also follows the same recommendations by the mentioned studies. The downstream positions for the outflow is set at $x/c > 0.8$ further than the observed transition location ($x/c > 0.5$) in the experiment at the lowest turbulent intensity. A mesh generator called *gridgen-c* developed by Sakov[17] is used to generate the mesh. The upper and lower bounds conform to the streamlines extracted from complementary Reynolds Averaged Navier-Stokes (RANS) computations. These RANS simulations have been performed for the wing installed inside the wind tunnel in accordance with the experiments.

2.3. Roughness induced crossflow vortices

The most unstable mode based on the linear stability theory as is reported in the experiment has a spanwise periodicity of 12 *mm* which is excited by an array of cylindrical roughness element. Numerically such periodicity can

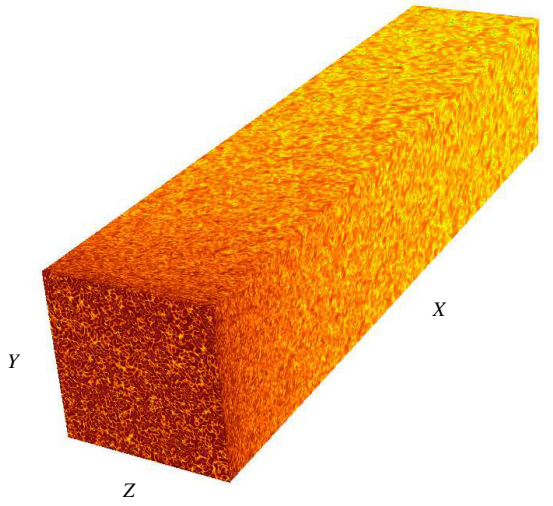

Fig. 2. A sample of the box used in the generation of the freestream turbulence. At the inflow, randomly superposed Fourier modes are added on top of a constant velocity. The top and bottom along with the lateral side have periodic boundary conditions. Isosurfaces of perturbation energy, drawn at $\pm 0.0001|v'|$. *X, Y, Z* are the cartesian coordinate systems.

be achieved by imposing periodic boundary conditions on lateral boundaries of the domain spaced at that specific periodic wavelength. The method has been successfully tested in the studies by Tempelmann et al.[16]. The roughness elements have a height of 12 μm and a diameter of 3 mm. The roughness shape is formed by displacement of the Gauss Lobatto Legendre (GLL) points normal to the surface.

2.4. Freestream turbulence

Different methods have long existed for generating freestream isotropic turbulence. One typical tool of generating freestream turbulence is through the Fourier periodic codes. One important aspect of using such codes is the continuous injection of energy into the periodic box. This maintains the spectrum as long as the energy injection rate and dissipation rate cancel out. Schlatter[18] gives an overview of such methods, and present relevant results for different cases. A very low level of freestream turbulence as is reported in the experiment, results in a very low Taylor's micro-scale Reynolds number (Re_λ). In other words the spectrum can be very viscous leaving a very narrow band for energy injection. For studies regarding such spectrums refer to Kerr[19], Mansour[20], Burattini et al.[21], and Ishihara et el.[22].

Another approach is to use a box with an inflow superposed by randomly superposed Fourier modes accompanied by periodic boundary conditions on the side walls with an outflow boundary condition at the outlet (see figure 2). The amplitude and Reynolds number are set such that the required Taylor's micro-scale and Reynolds number is achieved. Taylor's micro-scale is computed using the following relation

$$\lambda = \sqrt{5\frac{E_{tot}}{Ens}}, \tag{1}$$

where E_{tot} is the calculated integral energy at each streamwise plane, while Ens is the equivalent enstrophy value at those planes. The Taylor's Reynolds number is defined by

$$Re_\lambda = \lambda Re \sqrt{\frac{2}{3}E_{tot}}, \tag{2}$$

with Re denoting the Reynolds number of the simulation. The turbulent intensity is defined based on the r.m.s (root mean square) value of the vertical velocity component. The resulting perturbation field is then interpolated onto the wing mesh, in addition to interpolation in time using a third order Lagrange interplant.

Table 1. Turbulent characteristics of the simulated flow cases.

Case Name	Turbulent intensity	Integral length scale	Re_λ
Tu04	0.04%	12mm	1
Tu40	0.40%	12mm	20

In our set up we aim at finding the effect of freestream turbulence considering two of the cases as listed in Table 1. Turbulence intensities of 0.04% and 0.40% are chosen. There exist a difference in the Taylor Reynolds number which are selected as 1 and 20 respectively. The box has a total number of 128000 elements with an element order of ($N = 11$). A higher element order ($N = 13$) is also used in order to check the grid dependency. Figure 3a shows the comparison of the root mean square values of the perturbation velocities. A good level of agreement can be observed, indicating an isotropic turbulence field. The computed flow is now extracted given the desired intensities and length scales, and interpolated onto the grid of the wing geometry. Note the spanwise length is chosen equal to the spanwise periodicity of the roughness elements.

3. Results

3.1. Unsteady disturbances

Figure 4 shows the isosurfaces of the streamwise velocity for the two cases. It could be seen that the transition location shifts upstream as the level of freestream turbulence is increased by one order. Note that these values of freestream turbulence are reportedly at a very low range. The transition location shift could be better shown by looking at the time averaged friction coefficient in Figure 5a. A 10% shift in transition location is visible. In Figure 5b, the transition location from DNS is compared with those observed in the experiments. The roughness element has the same characteristics as in the experiment. It could be seen that there is a shift in transition location for similar turbulence intensities between experiment and simulations. The trend however seems to be consistent with the experiment and an increase in the turbulent intensity shows the same linear behavior.

Figure 6a shows the amplitudes of the stationary and non-stationary disturbances inside the boundary layer. The amplitude of the non-stationary disturbances are computed through a Fourier transform in time. The blue lines represent the unsteady perturbation of the higher turbulence intensity case as is clear from the figure. The explosive growth of the high frequency modes could be seen at around 0.5 x/c while similar explosive growth occurs later for the case with a higher turbulence intensity. The observed explosive growth is a classical signature of secondary instabilities which appear to be stronger for the case with higher turbulence intensity.

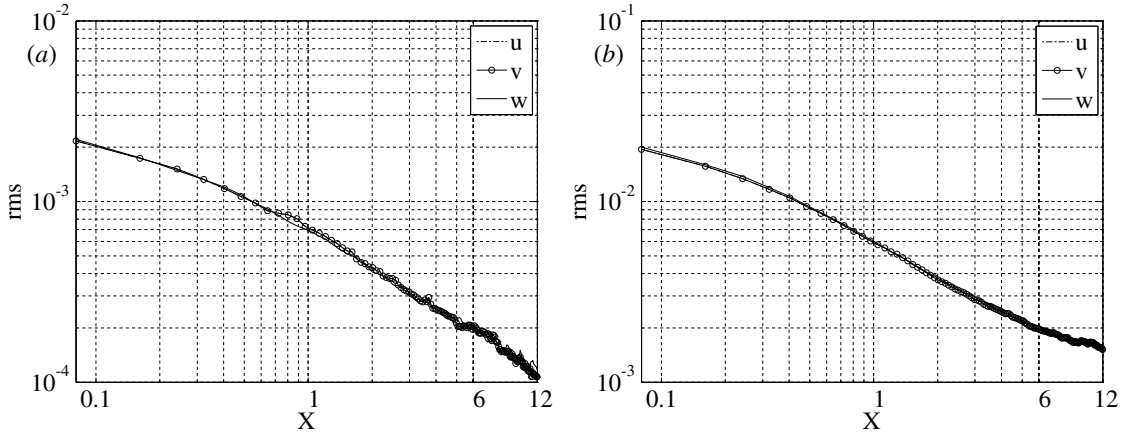

Fig. 3. Root mean square of velocity perturbations within the periodic box. (a) Tu04 and (b) Tu40.

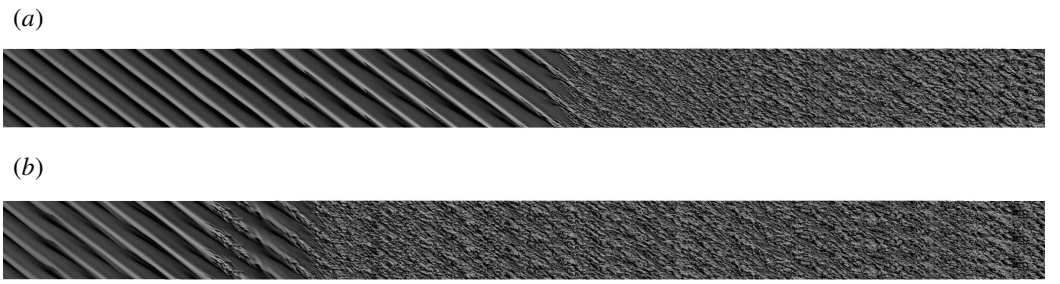

Fig. 4. Visualization of stationary crossflow vortices. The isosurfaces represent the streamwise velocity u. Three spanwise periods are shown for visualization purposes for (a) Tu04 and (b) Tu40

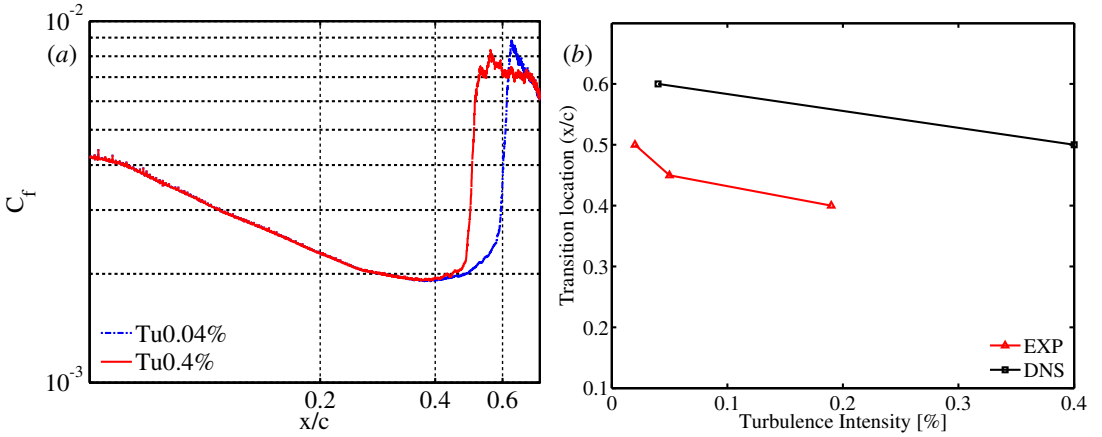

Fig. 5. (a) Time-averaged friction coefficient for the two cases with different turbulence intensities. (b) Transition location as a function of turbulence intensity.

Figure 6b shows the r.m.s. value of the streamwise velocity perturbations at $\eta = 7\delta$, along the chordwise direction. Here, δ is the boundary-layer thickness. It can be seen that the r.m.s. value for both cases saturates to a certain value after transition. It's interesting to note that the growth and the initial amplitude appears to behave linearly by increasing the turbulence intensity by one order. No additional receptivity mechanism could be seen other than the dominant one near the leading edge.

4. Conclusions

Direct numerical simulations (DNS) have been performed in order to investigate the role of freestream perturbations at a very low turbulence level on crossflow instability. The studied cases follow the experiments conducted by Downs et al. in Texas A&M University. In their experiment the authors document the freestream perturbations to a great detail, reporting freestream turbulence length scales, intensity, spectrum, etc. This enables the numerical studies to reproduce the freestream perturbations in such analysis. The experiment used ASU(67)-0315 wing geometry designed to promote crossflow instability. In our study we approach the reported values in generating the low intensity freestream turbulence. A DNS code (nek5000) has been used in order to generate the perturbation field. The perturbations are then interpolated onto the wing mesh.

Two different set of freestream turbulence characteristics have been chosen. It was observed that increasing the turbulent intensity by one order, while keeping the same integral length scale shows a linear behavior in terms of transition location. The receptivity mechanism also proved to be linear. It must be noted that the integral length scale was kept at constant value. Addition simulations investigating the effect of such a parameter while keeping

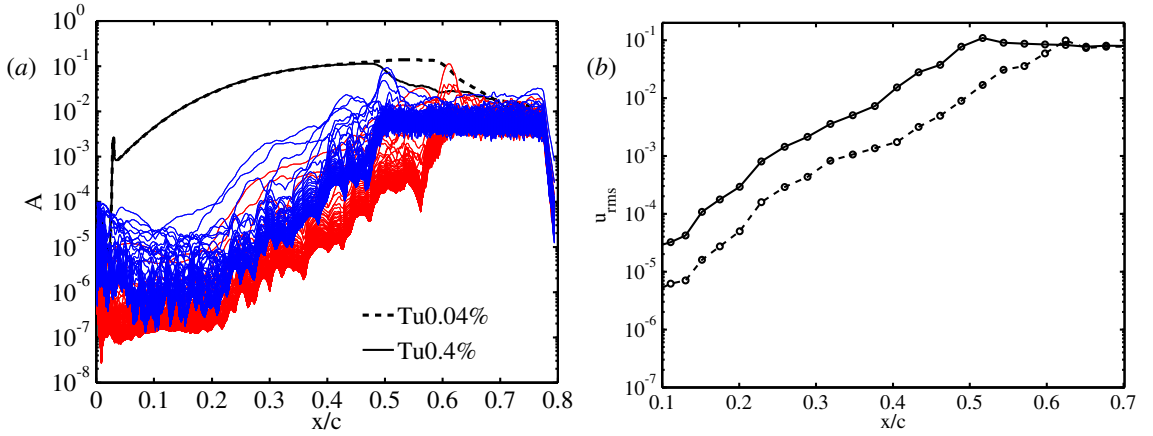

Fig. 6. (a) Amplitude of stationary and non-stationary perturbations inside the boundary layer. (b) The r.m.s. amplitude of the perturbation measured at $\eta = 7\delta$.

the turbulence intensity could shed additional light on the effect of low range freestream turbulence on crossflow instability.

Acknowledgments

The work reported here has been carried out within RECEPT project. This project has received funding from the European Unions Seventh Framework Programme for research, technological development and demonstration under grant agreement no ACPO-GA-2010-265094. All simulations has been performed at The National Supercomputer Centre in Sweden (NSC) with computer time granted by the Swedish National Infrastructure for Computing (SNIC).

References

1. M. Matsubara, P. H. Alfredsson, Boundary-layer transition under free-stream turbulence, J. Fluid Mech. 430 (2001) 149–168.
2. P. Jonáš, O. Mazur, V. Uruba, On the receptivity of the by-pass transition to the length scale of the outer stream turbulence, Eur. J. Mech B/Fluids 19 (2000) 707–722.
3. J. H. M. Fransson, M. Matsubara, P. H. Alfredsson, Transition induced by free-stream turbulence, J. Fluid Mech. 527 (2005) 1–25.
4. T. Kurian, J. H. M. Fransson, P. H. Alfredsson, Boundary layer receptivity to free-stream turbulence and surface roughness over a swept flat plate, Phys. Fluids 23 (2011) 034107.
5. S. Shahinfar, An experimental study on streamwise streaks in transitional boundary layer, Ph.D. thesis, KTH Stockholm (2013).
6. L. E. Hunt, Boundary-layer receptivity to three-dimensional roughness arrays on a swept-wing, Ph.D. thesis, Texas A&M University (2011).
7. R. S. Downs, Environmental influences on crossflow instability, Ph.D. thesis, Texas A&M University (2012).
8. R. G. Jacobs, P. A. Durbin, Simulations of bypass transition, J. Fluid Mech., vol. 428, pp. 185-212 428 (2001) 185–212.
9. C. E. Grosch, H. Salwen, The continuous spectrum of the Orr-Sommerfeld equation. Part 1. The spectrum and the eigenfunctions, J. Fluid Mech. 87 (1978) 33–54.
10. L. Brandt, P. Schlatter, D. Henningson, Transition in boundary layers subject to free-stream turbulence, J. Fluid Mech. 517 (2004) 167–198.
11. L. U. Schrader, S. Amin, L. Brandt, Transition to turbulence in the boundary layer over a smooth and rough swept plate exposed to free-stream turbulence, J. Fluid Mech. 646.
12. V. Ovchinnikov, M. M. Choudhari, U. Piomelli, Numerical simulation of boundary-layer bypass transition due to high-amplitude free-stream turbulence, J. Fluid Mech. 613 (2008) 135–169.
13. P. F. Fischer, J. W. Lottes, S. G. Kerkemeier, nek5000 Web page, http://nek5000.mcs.anl.gov (2008).
14. A. T. Patera, A Spectral Element Method for Fluid Dynamics: Laminar Flow in a Channel Expansion, J. Comp. Phys. 54 (1984) 468–488.
15. D. Tempelmann, A. Hanifi, D. S. Henningson, Swept-wing boundary-layer receptivity, J. Fluid Mech. 700 (2012) 490–501.
16. D. Tempelmann, L.-U. Schrader, A. Hanifi, L. Brandt, D. S. Henningson, Swept wing boundary-layer receptivity to localised surface roughness, J. Fluid Mech. 711 (2012) 516–544.
17. P. Sakov, gridgen-c - an orthogonal grid generator based on the crdt algorithm (by conformal mapping), http://code.google.com/p/gridgen-c/ (2011).
18. P. C. Shlatter, Large-eddy simulation of transition and turbulence in wall-bounded shear flow, Ph.D. thesis, Swiss Federal Institute of Technology (2005).

19. R. Kerr, Higher-order derivative correlations and the alignment of small-scale structures in isotropic turbulence, J. Fluid Mech. 153 (1985) 31–58.
20. N. N. Mansour, A. A. Wray, Decay of isotropic turbulence at low reynolds number, Phys. Fluids 6(2) (1994) 808–815.
21. P. Burattini, P. Lavoie, A. Agrawal, L. Djenidi, R. A. Antonia, Power law of decaying homogeneous isotropic turbulence at low reynolds number, Phys. Rev. E 73 (2006) 066304. doi:10.1103/PhysRevE.73.066304.
URL http://link.aps.org/doi/10.1103/PhysRevE.73.066304
22. T. Ishihara, T. Gotoh, Y. Kaneda, Study of high—reynolds number isotropic turbulence by direct numerical simulation, Annu. Rev. Fluid Mech. 41 (2009) 165–180.